ELSEVIER

Journal of Power Sources 108 (2002) 41–52

JOURNAL OF POWER SOURCES

www.elsevier.com/locate/jpowsour

Start-up analysis for automotive PEM fuel cell systems

M. De Francesco*, E. Arato

Dipartimento di Ingegneria Ambientale, Università di Genova, Via Opera Pia 15, 16145 Genova, Italy

Received 16 July 2001; received in revised form 16 November 2001; accepted 6 December 2001

Abstract

The development of fuel cell cars can play an important role in resolving transport problems, due to the high environmental compatibility and high efficiency of this kind of vehicle. Among the different types of fuel cells, proton-exchange membrane fuel cells (PEMFCs) are considered the best solution for automotive applications at the moment.

In this work, constructive criteria are discussed with the aim of obtaining a power generation module adaptable to a wide range of cars.

A particular problem in accomplishing the overall project is represented by the definition of the compressor system for air feeding. In this work, the design approach to the problem will be delineated: some options are reviewed and the best solution is analysed.

The transient response of the system (fuel cell and compressor) is investigated in order to optimise the start-up running through a model of a fuel cell stack and a compressor simulation.

The model and its results are proposed as a work procedure to solve the problem, by varying external conditions: in fact, to perform the system start-up under stable conditions, the air relative humidity and temperature must be maintained in a proper range of values.

The approach here presented has been utilised for the definition of the characteristics of the power module and layout of a middle-size hybrid city bus in the framework of a project promoted by the European Union.

Keywords: Start-up analysis; Proton-exchange membrane fuel cells; Fuel cell stack

1. Introduction

The increase in pollutant emission levels and the parallel development of environmental awareness have forced the automotive industry to study innovative solutions to improve the quality of the urban environment. The technical problem was approached, above all, by US researchers in the early 1980s and the solutions realised consisted of the control of the emissions of traditional vehicles (catalysers and particulate recovery systems).

This approach achieved a notable decrease in toxins, pollutants and irritant components, such as CO, NO_x and hydrocarbons. Following US laws, the European directives, which in fact only impose the catalytic conversion of emissions, also support the studies of non-pollutant vehicles.

At the moment, electric vehicles have the largest share of the low-pollutant vehicle market but their autonomy is still not sufficient for normal use and the area required for the batteries considerably reduces the usable space.

With the aim of obtaining vehicles with the intrinsic possibility of zero emissions, new solutions of the problem were examined and tested in the early 1990s.

One of the most promising technologies for obtaining the desired result is represented by fuel cells, where electrical energy is obtained by direct conversion of combustible. Industrial solutions using this electrochemical device in the automotive industry are the proton-exchange membrane fuel cells (PEMFCs), producing electrical energy at low working temperature with high efficiency [1].

Furthermore, these systems offer the best solution for reducing pollution to zero in city centres: the fuel, usually hydrogen, is burned producing only water. This solution bypass NO_x production problems, typically involved in traditional engines powered by hydrogen.

The definition of the general layout criteria of a fuel cell vehicle presented in this work follows a method that can offer great advantages in terms of assembling simplicity (possibility of endowing an existing car with a power module) and modularity but it shows some start-up problems. In fact, following this approach, the power generation is influenced by the performances of the motor of the compressor. In addition, the pressure inside the stack is furnished by the compressor and its motor is fed by the energy produced by the stack.

The need to examine the transient response of the fuel cell stack coupled to the air compressor has been resolved with a model of the transient behaviour of the system, developed on

* Corresponding author. Tel.: +39-10-353-6502; fax: +39-10-353-2589.
E-mail address: mdf@diam.unieg.it (M. De Francesco).

0378-7753/02/$ – see front matter
PII: S0378-7753(02)00003-4

Nomenclature

a	relative humidity, defined by Eq. (A.3)
C_p	mass specific heat (J kg^{-1} K^{-1})
D	diffusivity (m^2 s^{-1})
D_λ	diffusivity as a function of λ (m^2 s^{-1})
F	Faraday constant (C mol^{-1})
ΔG	Gibbs free energy change of the overall reaction (J mol^{-1})
ΔG_{st}	standard ΔG of the overall reaction (J mol^{-1})
h	heat transfer coefficient (W m^{-2} K^{-1})
ΔH	enthalpy change of the overall reaction (J mol^{-1})
I	electrical current density (A m^{-2})
I_0	exchange current density (A m^{-2})
k	hydraulic permeability of the membrane (m^2)
k_b	Boltzmann constant (J K^{-1} per molecule)
m	membrane thickness (m)
M	equivalent weight of membrane, i.e. weight of membrane per mole of SO_3^- groups (g mol^{-1})
M_t	total weight of stack (kg)
n	number of moles (mol)
n_e	number of electrons transferred in the reaction
p_i	partial pressure (Pa)
P	total pressure (Pa)
R	gas constant (J mol^{-1} K^{-1})
s_{air}	contact area air per cell (m^2)
s_{est}	external surface (m^2)
S	total internal cell surface (m^2)
t	time (s)
T	temperature (K)
V	potential (V)
V_s	inner stack volume occupied by air (m^3)
x	mole fraction
z	co-ordinate (m)

Greek letters

α	parameter defined by Eq. (A.5) (mol m^{-2} s^{-1})
β	charge transfer coefficient
β'	parameter defined by Eq. (A.6) (mol m^{-2} s^{-1})
χ	ratio net water flux through the membrane/water produced by the electrochemical reaction
δ	parameter defined by Eq. (A.8) (mol m^{-2} s^{-1})
Φ	coefficient in Eq. (10)
γ	parameter defined by Eq. (A.7) (mol m^{-1} s^{-1})
γ_1, γ_2, γ_3, γ_4	coefficients in Eq. (13)
η	overpotential (V)
φ_1, φ_2, φ_3, φ_4, φ_5, φ_6	coefficients in Eq. (A.4)
λ	ratio H_2O/SO_3^- in membrane
λ_0	value of λ at the cathodic side
λ_1	value of λ at the anodic side
θ	diameter of water molecule (m)
ρ	membrane density (kg m^{-3})
σ	resistivity (Ω^{-1} m^{-1})
τ	vapour pressure of water (Pa)
υ	stoichiometric coefficient
Ω	electrical resistance, Ω m^2
ξ	parameter defined by Eq. (A.9) (m^{-1})
ψ_1, ψ_2, ψ_3, ψ_4	coefficients in Eq. (A.2)
ζ	electro-osmotic drag coefficient

Subscripts

a	anode
c	cathode
air	air
est	external stack surface
exp	experimental
ext	external to the stack
H_2O	water
O_2	oxygen
stack	stack
u	total number of moles
343	evaluated at temperature of 343 K

Superscripts

0	initial conditions
c	cell
el	electrode
ls	losses
memb	membrane
t	thermodynamic

the basis of experience acquired through the participation of the group of University of Genoa in the European project for the development of a middle-size city bus.

In general, at high values of temperature and relative humidity the power furnished by the fuel cell stack (strongly dependent on these variables) is sufficient to move the motor of the compressor; moreover, the transient model of the entire system allowed us to analyse some running options and to determine the best solution for the start-up of the ''power module system''.

2. General description of a fuel cell vehicle

The solution here proposed for the realisation of a fuel cell vehicle can be considered an innovative approach to the problem.

In fact, hybrid fuel cell vehicles [2] are usually realised by coupling an electric power generator to a battery storage system. The surplus energy is stored and utilised when the electric motor needs peak power.

In the solution proposed here, the power generator is utilised only to charge the batteries which feed the engine of the bus. In addition, two alternative solutions for the

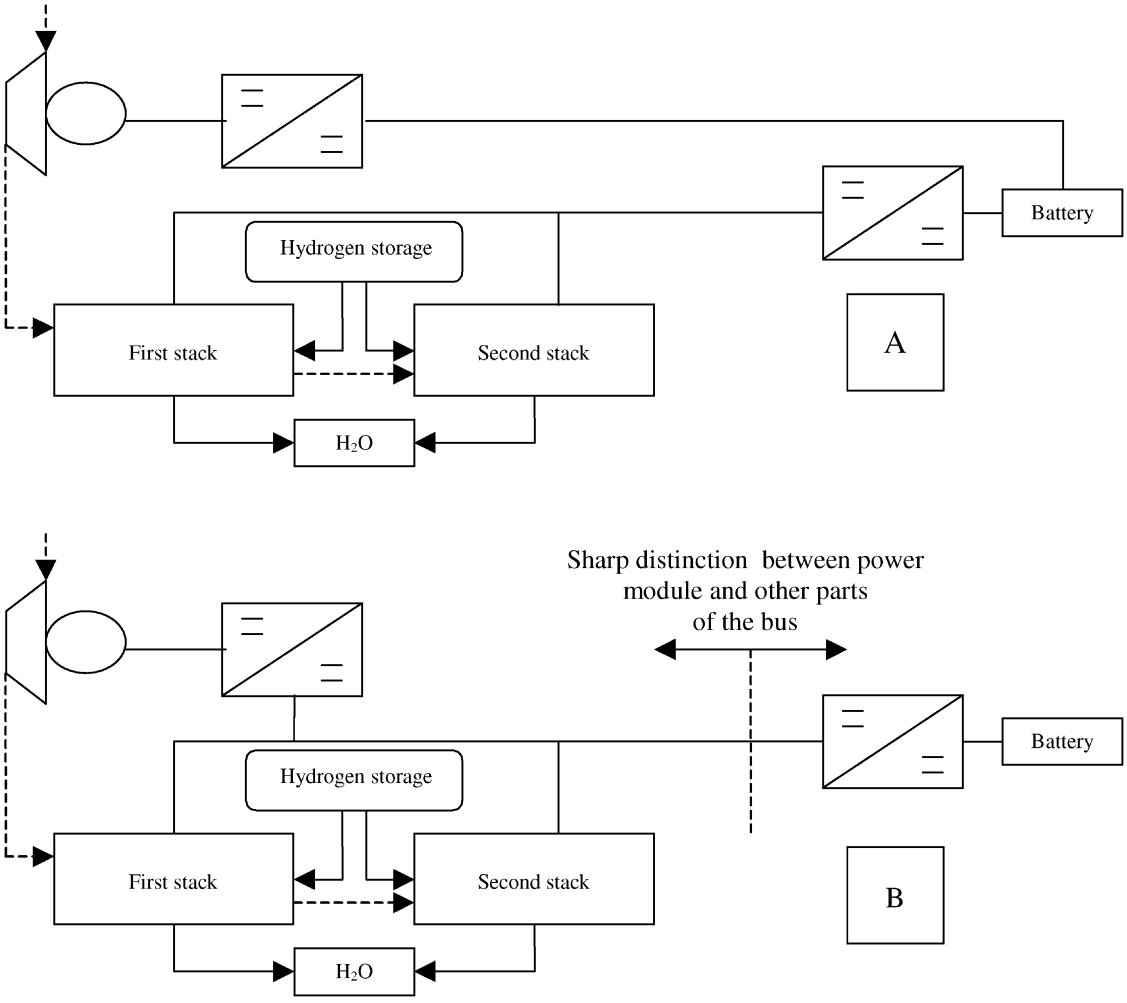

Fig. 1. Two alternative working schemes for the whole motor + compressor.

energy supply to the motor of the compressor are reviewed: Fig. 1A represents the "traditional" approach, feeding the motor from the batteries [2]; Fig. 1B represents the novel approach where the motor of the compressor is fed by the power generator.

A hybrid fuel cell vehicle designed following the latter approach can be divided into two distinct sections: the first section consists of the chassis with steering, batteries, electric motor, braking system and electronic control centre for all equipment and the second one is represented by the energy generation system, consisting of one or more fuel cell stacks and auxiliaries (air compressor, hydrogen or other fuel feeder, heat exchangers, dc/dc converter and a maximum power point tracker to feed the batteries). The scheme of the bus reported in Fig. 2 highlights the innovative approach.

The modularity of the system permits the construction of a pack independent of battery characteristics, in agreement with the typical modular concept of fuel cells. Following this criterion, it is possible to use any chassis as a base, making sure to put the electrical generation system in an autonomous chassis connectable to the principal one.

2.1. Fuel cell power generator

PEMFCs are actually considered the best solution for automotive applications [1]. This is due to criteria related to the flexibility of their use (starting is very simple, the device is of small dimensions, efficiency is very good) and the low working temperature, which is important for the intrinsic safety of the vehicle.

These cells are formed of a perfluosulfonic membrane as electrolyte coupled with two electrodes (anode and cathode) built utilising a substrate of carbon–PTFE coated with platinum as electrocatalyst.

Air is fed to the cathodic compartment while hydrogen is fed to the anodic one and the electrolyte performs both the functions of transferring H^+ from the anode to the cathode and reactant separation.

Electrochemical reactions involved are:

$$H_2 \rightarrow 2H^+ + 2e^- \quad \text{(anode)}$$

$$2H^+ + \tfrac{1}{2}O_2 + 2e^- \rightarrow H_2O \quad \text{(cathode)}$$

$$H_2 + \tfrac{1}{2}O_2 \rightarrow H_2O \quad \text{(overall reaction)}$$

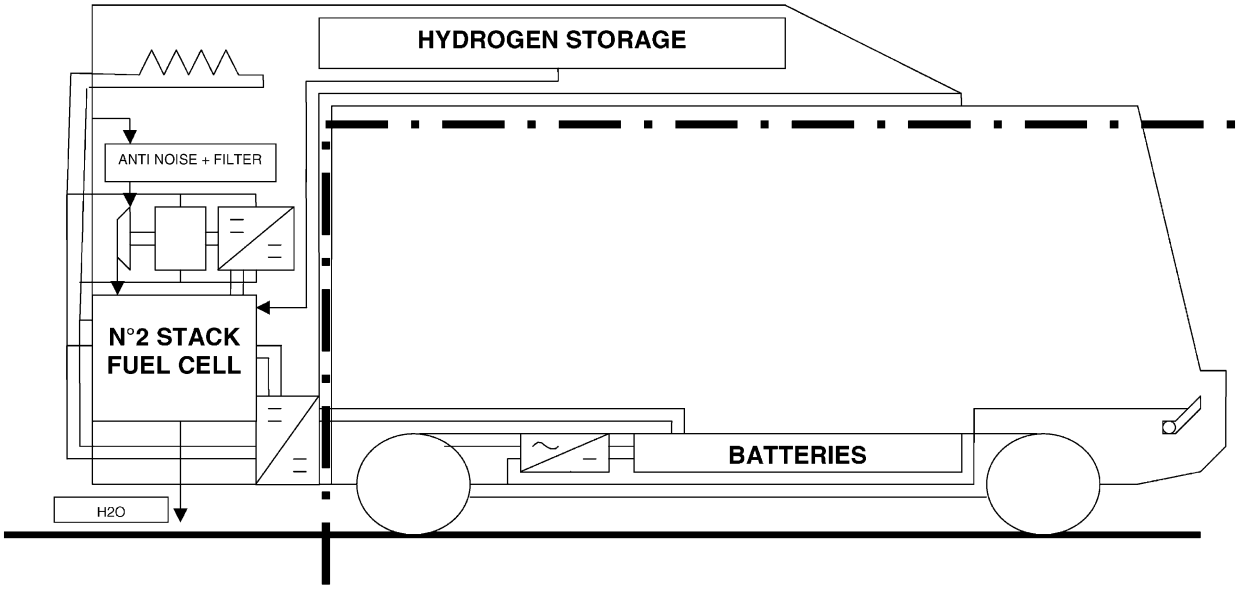

Fig. 2. General scheme of a hybrid fuel cell bus.

Stacks are obtained by connecting a number of cells in series while gas distributors (the bipolar plates) accomplish the function of feeding the fuel to the anodic side and air (or oxygen) to the cathodic one.

Using common relationships between the power continuously supplied by the generation module and that adsorbed by the vehicle and paying particular attention to one of the possible urban cycles—in this case represented by Cole's relationship [3]—the peak power requested by a middle-size city bus can be considered about 100 kW, while the power consumed by the auxiliary systems, including all the losses, can be estimated at about 10 kW. So, the battery design is based on the maximum power needed by the whole system (bus and auxiliaries). As a consequence, to guarantee continuous bus running, the installed power furnished by the fuel cells must be about 50 kW [4].

In this case, the choice of the low power installed in the bus is due to economical reasons in the development of the prototype. In addition, due to the characteristics of the modularity of this solution, the results obtained will be adaptable to a wide number of automotive realisations (cars and buses).

2.2. Reactant feeding system

The supply of fuel (H_2) to the cells is usually a simple operation from the point of view of the regulation of the pressure and flow rate. In fact, the gas is contained in one or more cylinders on the roof of the vehicle and through valve control it is possible to obtain the characteristic desired.

On the contrary, the supply of air is not so straightforward: it is necessary to feed a constant air flow rate with a very high purity level to avoid poisoning the fuel cells.

So, the possible options connected with the choice of the air compressor system refer to working pressure, air purity and system layout.

Literature data on the fuel cell power supply [5] show the best performances for high air pressure, but to get a simple constructive solution and management, low working pressure has been chosen: the decrease in electrical performances is compensated by the simplicity of the system and the containment of costs.

With regard to the problem of air purity, the solution that guarantees the complete absence of dragged oil or metallic shards is represented only by an oil-free screw compressor. This solution offers all the advantages of the rotative compressors without wear, drag and eventual abrasion of moving parts. The lack of wear is achieved thanks to two rotors with low but sufficient tolerances to guarantee no contact. High rotational velocity (about 30,000 rpm) provides the chosen working pressure in only one stage. The characteristic curves of the compressor installed in the bus are reported in Fig. 3: the solid line represents the power needed by the compressor as a function of its rotation speed; the broken line the air flow rate and the dotted line the adiabatic efficiency. The maximum adiabatic efficiency is reached when the compressor works at 60% of the nominal power.

In the layout of the air feeding system described earlier (Fig. 1B), all the devices present in the power module can only take energy from the electrochemical generator.

3. Simulation of the power module

A wide number of works [6–12] demonstrate that the starting of PEMFCs is instantaneous, but practically no information is available on the start-up problems of the entire power module system (stack + compressor + motor). To analyse the transient behaviour, study the influence of environmental conditions and determine the best start-up path

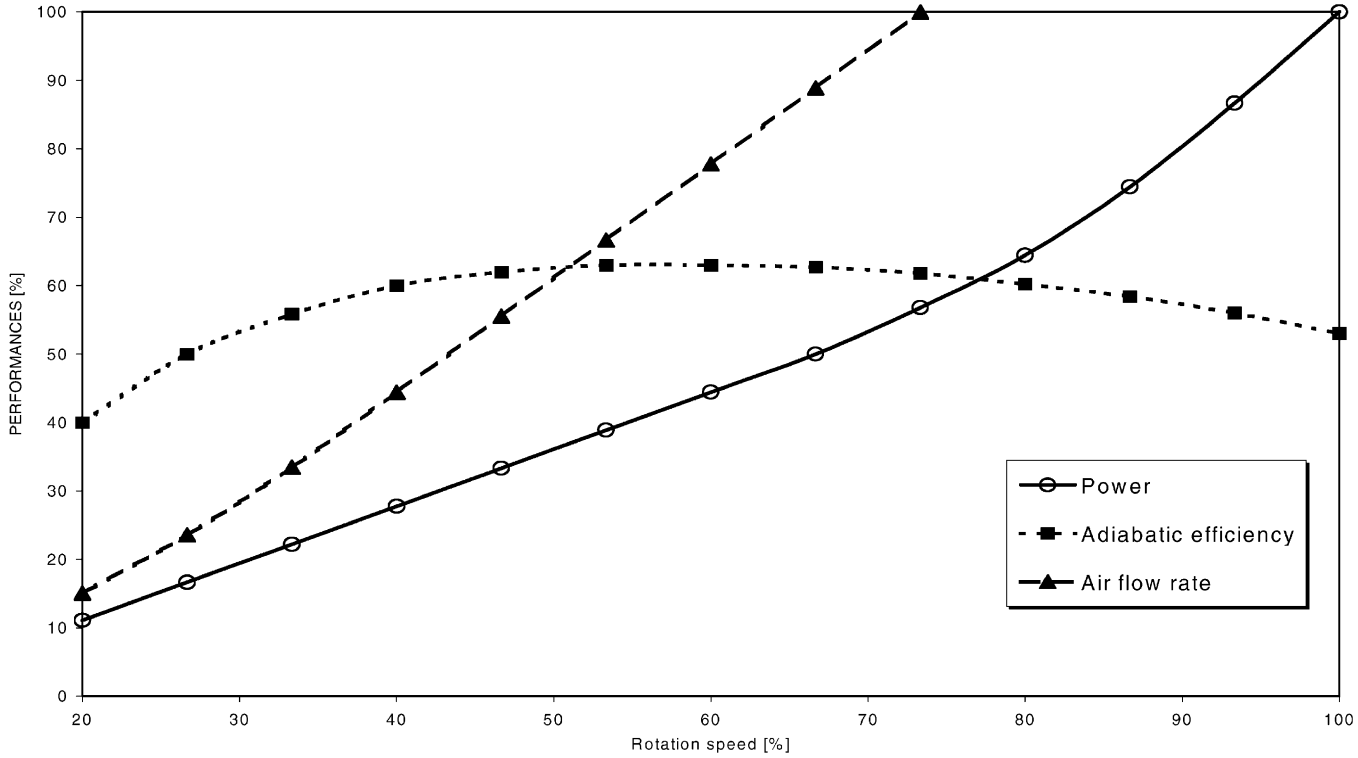

Fig. 3. Typical Lysholm screw compressor performances.

without operating fuel cell devices under limit conditions, a simulation model of the power module system was set up.

The simulation of a power module includes both the model of the fuel cell stack and the experimental trend of the compressor and of the motor system. This "mixed" approach is motivated by the need to predict the stack operative conditions that will avoid damaging drying or flooding of the membrane.

3.1. Stack simulation

Theoretical approaches [7,8,11–14] have often been developed under steady state conditions and in general are not able to describe fuel cells coupled with an external utilisation.

This work presents a dynamic study of an electrochemical device which includes a macroscopic simplified fuel cell model coupled with a detailed description of the membrane. This tool furnishes, in reasonable time, a satisfactory description of the stack behaviour comparable with experimental literature data and more complex approaches.

The main assumptions of the model are:

- uniformity of the stack temperature;
- hydrogen exiting from its bottle instantaneously reaches the stack temperature (this is due to the low hydrogen specific heat);
- momentum balance is substituted by the experimental data obtained from a screw compressor coupled with a fuel cell stack simulator;
- operating conditions far from diffusion limiting ones.

The time-dependent equations of the model are written in a macroscopic form and in order to have a fast numerical integration including mass balances inside the cell and the energy balance of the solid.

Cell voltage is calculated taking into account activation overpotential, Ohmic effects and diffusive limitations. Then, the results of a single fuel cell have been extended to an entire stack considering this formed by a number of cells with the same properties.

The time-dependent that assume the feeding pressure of the hydrogen constant for every operative condition, are reported in the following:

- for water

$$\frac{\partial n_{H_2O}}{\partial t} = \frac{I}{n_e F} S \quad \text{if } a < 1 \tag{1}$$

or

$$\frac{\partial n_{H_2O}}{\partial t} = 0 \quad \text{if } a \geq 1 \tag{2}$$

with initial conditions:

$$\text{for } t = 0, \quad n^0_{H_2O} = \frac{p^0_{H_2O}}{P^0} n^0_u \tag{3}$$

- for oxygen

$$\frac{\partial n_{O_2}}{\partial t} = -\frac{IS}{2n_e F}; \tag{4}$$

with initial conditions:

$$\text{for } t = 0, \quad n_u^0 = \frac{P^0 V_s}{RT} \text{ and } n_{O_2}^0 = n_u^0 x_{O_2}^0 \tag{5}$$

Some considerations are necessary for the interpretation of the energy balance of the solid. The evaluation of start-up effective strategies are evaluated under safe conditions, i.e. under the worst conditions for the whole system: absence of external coolant/heating, heating by feeder gas only during the steady state compression phases, absence of forced humidification.

For these reasons, the energy balance is interpreted as a time-dependent equation that relates stack temperature variations to the heat losses and the exchanges with the air flow and the environment:

$$M_t (C_p)_{stack} \frac{\partial T_{stack}}{\partial t} = h_{air} s_{air} (T_{air} - T_{stack}) + h_{est} s_{est} (T_{ext} - T_{stack}) - \left(\frac{\Delta H}{n_e F} + V^c \right) IS \tag{6}$$

The water condensation in the energy balance has been neglected because the term of condensation enthalpy is negligible if compared with the others. Heat transfer coefficients are evaluated as that of the forced air for the inner side and the natural convection for the external one, following Amphlett et al. [6]. For the same reasons as discussed above no coolant or heater are present.

The calculation of the Nernst potential (V^t):

$$V^t = \frac{-\Delta G}{n_e F} = \frac{-\Delta G_{st}}{n_e F} - \frac{RT}{n_e F} \ln \left(\prod_i p_i^{\upsilon_i} \right) \tag{7}$$

is the basis for the evaluation of the energetic performances of the single cell.

In fact, in the PEMFCs the open circuit voltage does not correspond to the Nernst voltage: this is due to parasitic phenomena, such as undesirable electrochemical reactions at the cathode which produce an overpotential that is evaluated as a constant value in accord with Rho et al. [11]:

$$\eta^{ls} = 0.2V \tag{8}$$

following Bernardi and Werbrugge [13] and Springer et al. [14]:

$$\eta^{el} = \frac{RT}{\beta F} \ln \left(\frac{I}{I_0} \frac{P}{p_{O_2}} \right) \tag{9}$$

where the ratio P/p_{O_2} includes the concentration overpotential and I/I_0 the activation one.

Exchange current density (I_0) is evaluated following Anderson et al. [15]:

$$I_0|_T = I_0|_{343} \exp \left[\Phi \frac{T - 343}{343T} \right] \tag{10}$$

Then, the evaluation of the overall Ohmic effects in the membrane using a monodimensional model follows Springer et al. [14,16]: Ohmic losses are expressed as a function of the internal membrane humidity (λ), this related to the total current and the water contained in the active sites of the membrane (SO_3^- for a perfluosulfonic membrane).

The membrane Ohmic losses are:

$$\eta^{memb} = \Omega I \tag{11}$$

where the Ohmic membrane resistance is calculated along the membrane, by the integration of the conductivity:

$$\Omega = \int_0^m \frac{dz}{\sigma} \tag{12}$$

Eq. (12) is utilised by considering the conductivity taken from experimental evidence (Appendix A), as a function of the ratio between the water and the SO_3^- in the membrane and the mean temperature:

$$\sigma = (\gamma_1 \lambda - \gamma_2) \exp \left[\gamma_3 \left(\frac{1}{\gamma_4} - \frac{1}{T} \right) \right] \tag{13}$$

where λ is conditioned by the electro-osmotic drag, current density and pressure gradient between the two electrodic sides:

$$\frac{\partial \lambda}{\partial z} = \lambda \left(\zeta \frac{I}{n_e F} \frac{M}{\rho D_\lambda} - k \frac{3\pi\theta}{k_b T} \frac{P_c - P_a}{m} \right) - \chi \frac{I}{n_e F} \frac{M}{\rho D_\lambda} \tag{14}$$

Taking into consideration that diffusivity (D_λ) can be considered constant when no limiting current is reached [14], Eq. (14) can be integrated analytically to obtain an explicit form of Ohmic resistance (Appendix A):

$$\Omega = \frac{\exp[\gamma(T)][f(\xi, m)]\{\xi m - \ln[(\gamma_1 \lambda_1 - \gamma_2)(\exp(\xi m) - 1)] + \ln[f(\xi, m) g(\lambda_0)]\}}{\xi[\exp(\xi m) g(\lambda_0) - \lambda_1 \gamma_1 + \gamma_2]} \tag{15}$$

The effective voltage can be calculated considering the main losses.

Losses occurring at the cathode are mainly due to activation effect and they are of one order of magnitude higher than the overall anodic overpotential [12]: so, anodic overpotential will be neglected. Cathodic activation overpotential and concentration overpotentials have been calculated As evidenced in Eq. (15) Ohmic resistance is conditioned by the relative humidity of the reactants (λ_0 and λ_1).

Then, the cell voltage is expressed by:

$$V^c = V^t - \eta^{ls} - \eta^{el} - \eta^{memb} = f(I) \tag{16}$$

The model is integrated following two paths. In the former, able only to give a static interpretation of the stack

Table 1
Parameters of the simulation model

Parameter	Value
$I_0\|_{343}$	0.9 A m^{-2}
P^0	1×10^5 Pa
Φ	35000
γ_1	0.58 Ω^{-1} m^{-1}
γ_2	0.50 Ω^{-1} m^{-1}
γ_3	1268 K
γ_4	303 K
φ_1	5.1×10^{-10} m^2 s^{-1}
φ_2	-6.6×10^{-11} m^2 s^{-1}
φ_3	5.3×10^{-12} m^2 s^{-1}
φ_4	-1.3×10^{-13} m^2 s^{-1}
φ_5	2416 K
φ_6	303 K
ψ_1	0.043
ψ_2	17.81
ψ_3	−40
ψ_4	36
η^{ls}	0.2 V
β	2.9×10^{-1} kPa s^{-1}

power as a function of external conditions (temperature and relative humidity), the method of finite differences has been adopted. In the latter, where it was necessary to interpret the transient response, finite differences were coupled with a relaxation method for time-dependent equations.

The code is written in FORTRAN language and the resulting software runs on a personal computer in less than a minute.

The characteristic curve of a PEM commercial stack which consists of 100 cells (surface about 0.25 m^2 per cell) is evaluated for average cell temperature ($T = 343$ K, $p_{air} = 3.5 \times 10^5$ Pa, $p_{H_2} = 4 \times 10^5$ Pa and $a = 0.99$) utilising the parameters reported in Table 1; then the result referred to the single cell is reported in Fig. 4 to be compared with experimental data reported in literature [5,12] obtained under the same conditions.

The model contains simplifications that produce a 5% difference in the electric response of the stack compared to the results of other more elaborate models but the differences obtained by comparing the proposed model with some experimental results [8,11,12] are of the same magnitude obtained by applying the other models to these data [6–8,11,12,14,16]. This result confirm the validity of the model presented in this work.

The simplifications provide an analytic solution for the Ohmic overpotential that significantly reduces the computation time which decreases dramatically from 10 min for the calculation of only a point of electrical response (*I–V*) to a few seconds for the evaluation of the entire electrical curve.

In addition, the electric response of the stack has been calculated in different conditions of external temperature and air relative humidity: as can be seen in Fig. 5, the power generation is strongly dependent by these two variables.

Power values are represented as a percentage, considering 100% that is furnished at $T = 343$ K and 100% of relative humidity (about 30 kW).

The velocity of execution of the model permit its use to follow the transient behaviour of a complex system coupling the obtained results with the experimental trends of the compressor.

3.2. Compressor and motor experimental trends

To accomplish the simulation of the power module and to analyse the start-up of the whole system, the power needed

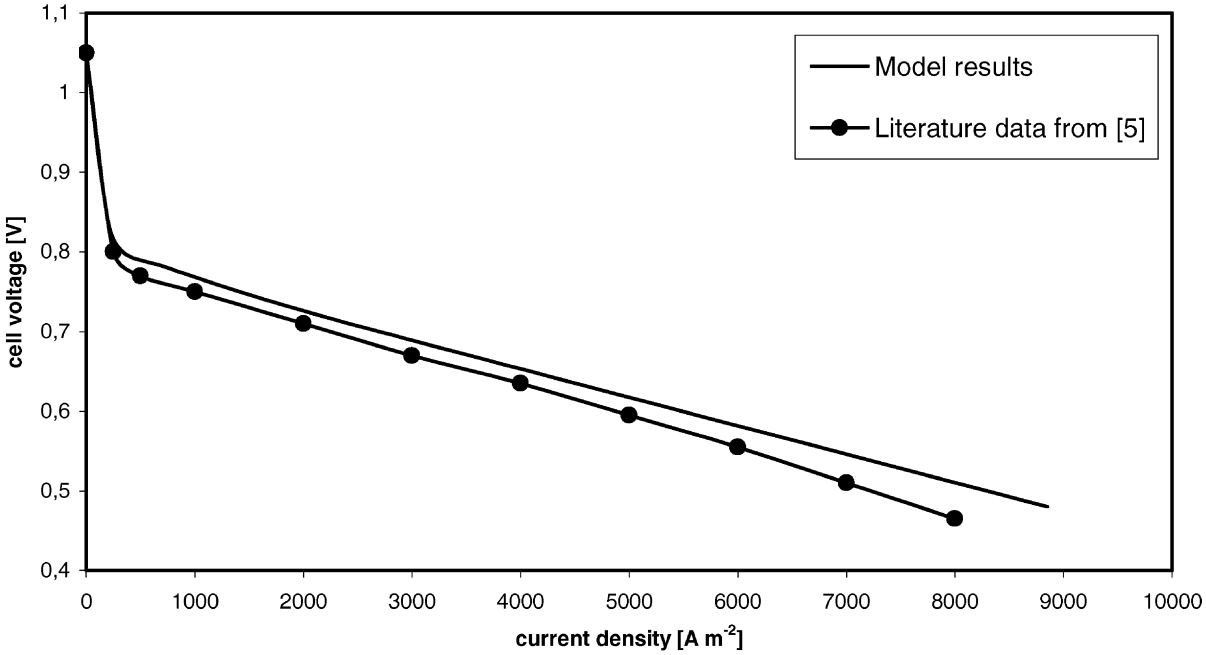

Fig. 4. Comparison between results and experimental literature data obtained under the same operating conditions.

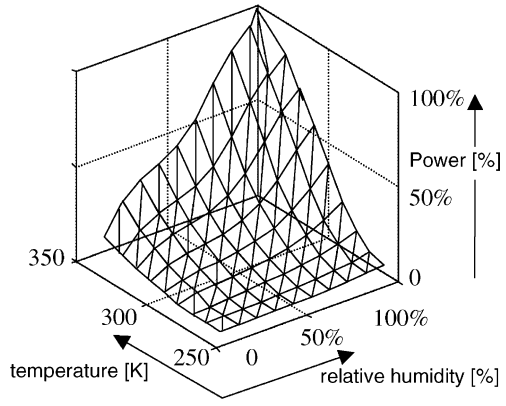

Fig. 5. Stack model output: results of power generation as a function of temperature and relative humidity.

by the motor of the compressor must be known. These data have been collected through participation in the European organisation for the construction of a middle-size city bus.

Experimental data were obtained in an industrial laboratory using a procedure that involved the connection of a screw compressor, fed by a motor, to a simulator of exhaust loss (a cylinder, with a calculated number of tubes passing through it, through which air was forced) designed to the specifications of a 30 kW fuel cell stack.

The motor was fed by an external connection. Some sensors were positioned to measure: power adsorbed by the motor, pressure in the mean and at the end of the stack, temperature and air flow rate at the compressor escape flange.

Measures were recorded by connecting all the sensors to an oscilloscope Tektronix model TDS 420A and all data were obtained in graphic format as a function of the rotations of the motor.

All device characteristics that were measured when the stack valves were opened, are reported in Fig. 6.

So, the power requested by the motor is composed with that produced by the fuel cell stack to individuate the possible start-up strategies.

The values of air temperature at the outlet of the compressor are utilised for the evaluation of the stack heating during transients, so the pressure values in the stack are available and when the stack is connected to the compressor, these data permit the calculation of the pressure in the stack introducing the experimental pressure data (P_{exp}):

$$P(t) = P_{exp}(t) + \int_0^t \left(\frac{\partial n_{O_2}}{\partial t} + \frac{\partial n_{H_2O}}{\partial t} \right) \frac{RT}{V_s} \, dt \quad (17)$$

In this way the transient stack model is coupled with the motor + compressor response to obtain the transient behaviour of the whole power generator module.

4. Discussion of start-up criteria

Four start-up strategies have been investigated utilising the model described above.

In the first it is considered that during the motor start-up (from 0 to 235 ms) air contained in the stack is not fed by the compressor flow. Air pressure and oxygen concentration vary as a function of the total energy furnished to the motor (including losses). Steady state is reached when the time is greater than 235 ms: only after this time, do pressure and oxygen concentration become equal to the equilibrium

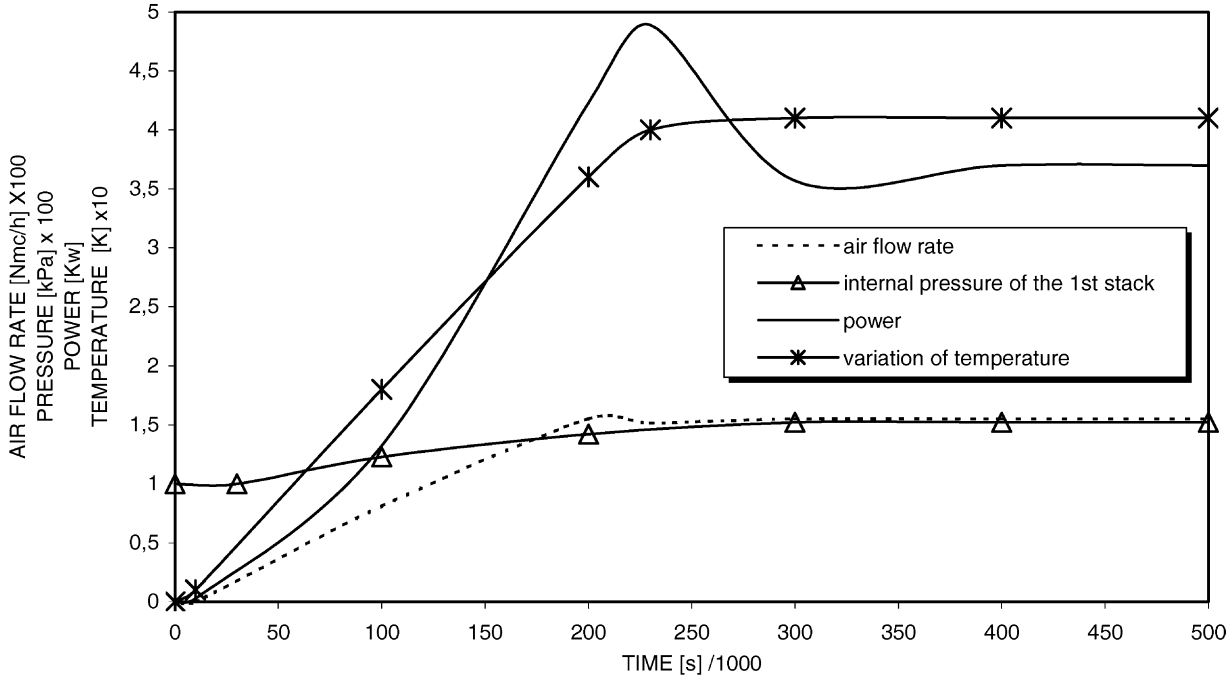

Fig. 6. Motor–compressor start-up behaviour.

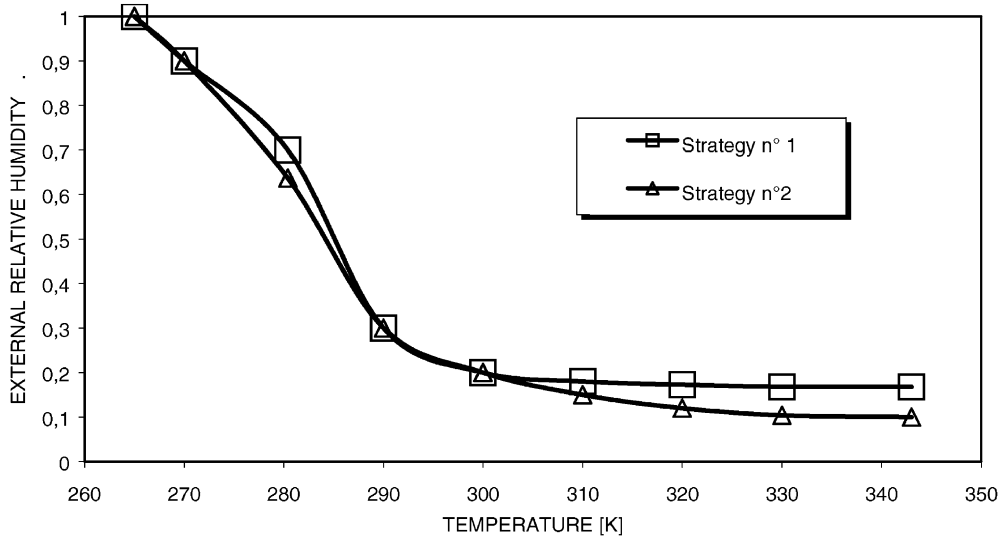

Fig. 7. Temperature and relative humidity start-up limits for strategies no. 1 and 2. Above the two lines, start-up can be realised. Below the two lines, start-up cannot be reached without humidification or without heating the stack.

conditions, considering the experimental values for the stack out of line with the internal consumption.

The second strategy considers that air pressure on the stack follows the experimental values; oxygen concentration is evaluated as above.

The start-up can be realised in safe conditions only when the power furnished by the cell is greater that those utilised by the motor of the compressor in all the early stages. Fig. 7 highlights the start-up limits of these two solutions.

In the third simulation strategy, a multi-step heating has been considered: the motor reaches the maximum power after the path described in Fig. 8; during the steady state, the stack is heated by reactions and gas heat. In the transient period the system is simulated in the same way as the first strategy.

In all the three former solutions, it is supposed that the humidifier is absent: results are conservative and discriminate external conditions.

The fourth solution is analogous to the third but relative humidity is maintained $\geq$50%, utilising an external humidifier. The results of the two latter strategies are reported in Fig. 9, realised in the same way as Fig. 7.

The simulation shows that the novel approach of Fig. 1B can be adopted and through the simulation of a stack in the absence of a humidifier, the operative limits of the solutions are identified (i.e. external temperature and air relative humidity).

The start-up can be realised "self-consistently" (i.e. utilising only the energy produced in the power module)

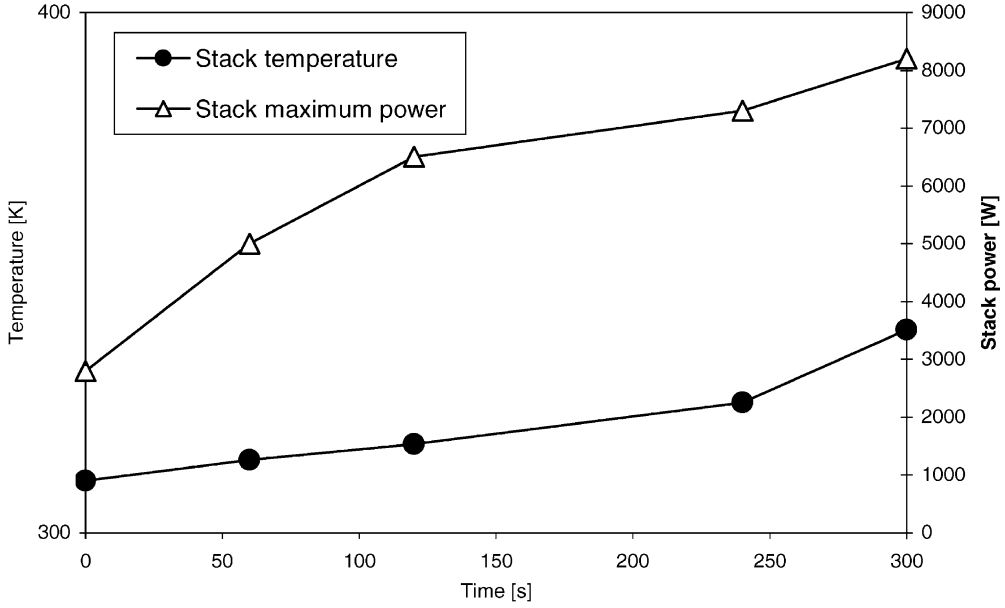

Fig. 8. Analysis of strategy no. 3: stack temperature and maximum power furnished during the analysed transient period.

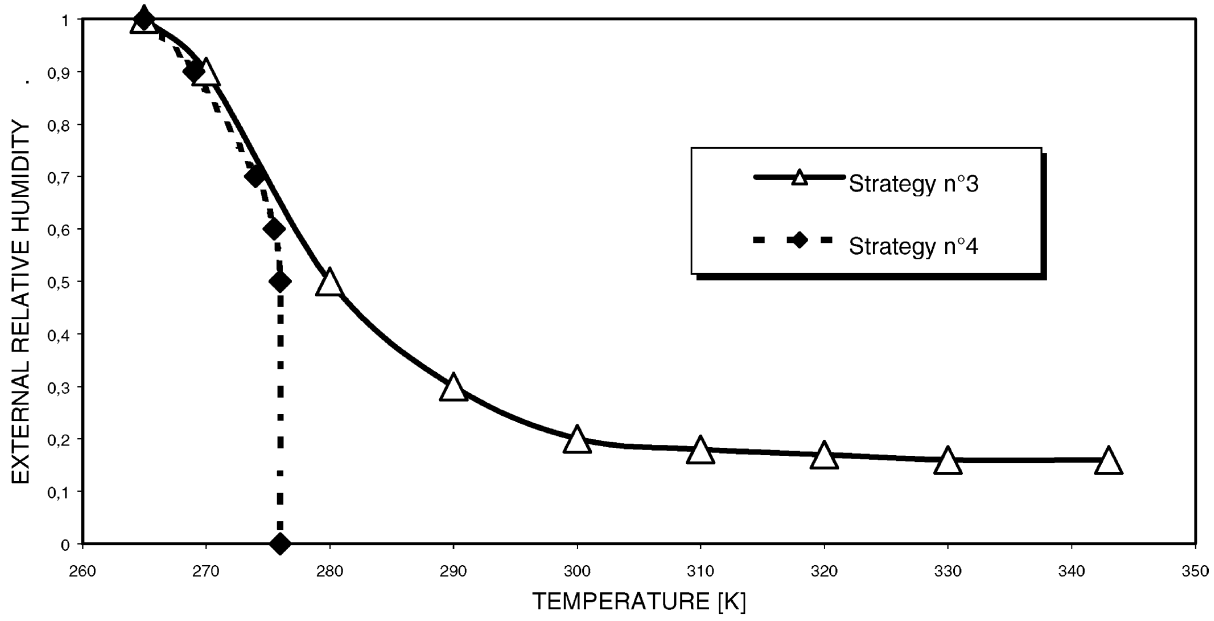

Fig. 9. Temperature and relative humidity start-up limits for strategies no. 3 and 4. Above the dotted line, start-up can be realised maintaining humidity >50%. Below the solid line, start-up cannot be reached without humidification or without heating the stack.

in a wide range of conditions. In spite of this result, the analysis of the trend of temperature and air humidity in the stack after the early running stages shown in Fig. 10 indicates that the air humidifier is essential after the start-up.

The presence of the air humidifier is also necessary to avoid the membrane drying out. In fact, when drying occurs the polymeric film can be broken and the cell damaged irremediably.

This work, however, shows the existence of climatic conditions favourable to start-up without humidifier. In fact, for $T = 293$ K and $a > 50\%$ (a typical weather condition of southern Europe), the air humidification is not necessary for the start-up.

Contrarily, for climatic conditions that can be frequent in northern Europe ($T = 273$ K, $a < 40\%$) the system needs the humidifier and also an air heater.

This consideration demonstrates that the design of the power module utilising the proposed novel approach can be successfully realised considering climatic conditions where the application will work.

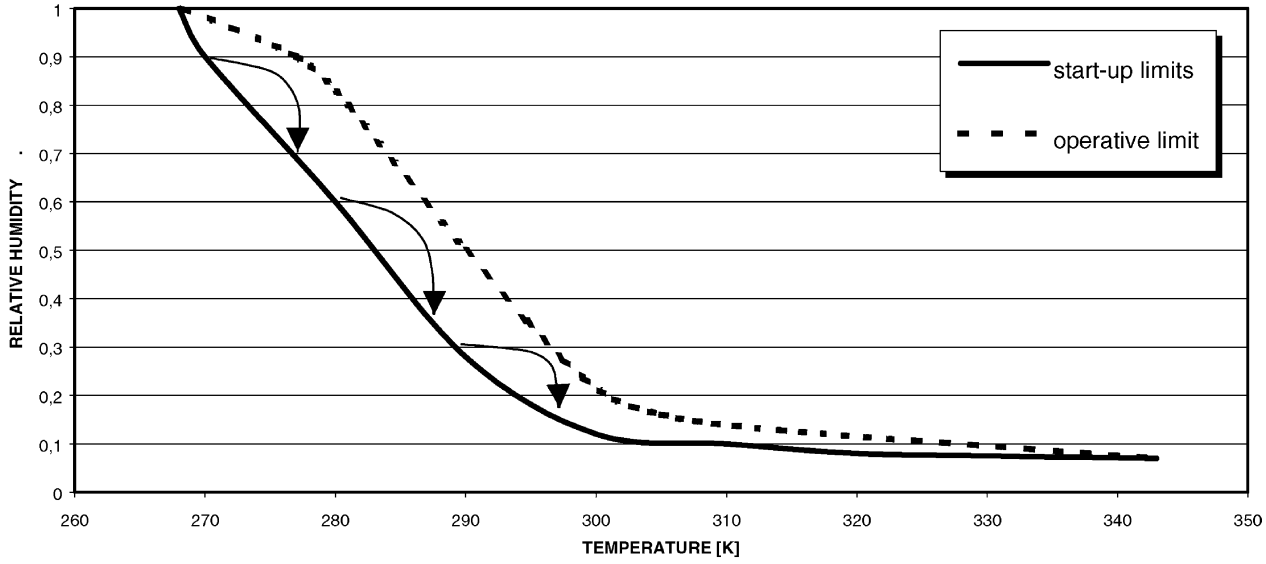

Fig. 10. Start-up operative limits. Solid line represents the external limit conditions for start-up in the absence of air humidification. Temperature and humidity in the stack start from the values represented by the solid line and follow the paths identified by the arrows. When the arrows reach the solid line, the power module is not able to sustain itself: above the broken line, obtained by matching the final values of temperature with the initial humidity ones, the system cannot operate without air humidification or stack cooling.

5. Conclusions

The planning of a non-conventional hybrid bus is an engineering theme of great importance. The design approach of the European team has shown that the possibility of successfully constructing a working vehicle is dependent on finding solutions not commonly espoused in the automotive world, even for accessories.

In this work, we have presented an innovative solution of a ''power module'' fuel cell pack independent of the vehicle. In particular, the start-up of this modular solution is strongly conditioned by the air compression system, which has been shown to be critical when its motor is fed directly by the electrochemical generator.

In addition, the choice of this device is not simple, given the restrictions on the particular characteristics of air purity the stacks require.

The course followed, however, permitted us to define a procedure that rationalised the analysis of the power module under study, with particular attention to the start-up problems of the system and the need to implement some auxiliaries (i.e. air humidifier and air heater).

Acknowledgements

This work has been partially supported by the European Union through the contract for the development of a full-size fuel cell city bus (ref. UE: JOE 3-CT 96—0043). In particular, we would like to thank the following companies: Air Technologies (Toulouse, France) and DTA-Air Liquide (Sassenage, France) for their contribution to the experiments; Nuvera (Milan, Italy) for supplying details of the fuel stacks; Opcon Autorotor (Nacka, Sweden) for supplying details of the screw compressor.

Appendix A

Following Springer et al. [14], membrane overpotential is hardly conditioned by the membrane hydration, which depends on the electro-osmotic drag due to the proton crossing the membrane in solvated form, water diffusion due to the non-uniform value of λ and pressure gradient. Eq. (14) includes these aspects.

Boundary conditions of Eq. (14) consider the evaluation of the surface humidity as a function of the external one:

$$z = 0, \qquad \lambda = \lambda_0 \tag{A.1}$$

where λ is that expressed by:

$$\lambda = \psi_1 + \psi_2 a + \psi_3 a^2 + \psi_4 a^3 \tag{A.2}$$

and

$$a = \frac{p_{H_2O}}{\tau} \tag{A.3}$$

The integration of Eq. (14) is difficult and this is due to the fact that diffusion has been expressed by Springer et al. [14] as a function of λ:

$$D_\lambda = (\varphi_1 + \varphi_2\lambda + \varphi_3\lambda^2 + \varphi_4\lambda^3) \exp\left[\varphi_5\left(\frac{1}{\varphi_6} - \frac{1}{T}\right)\right], \quad \lambda > 4 \tag{A.4}$$

The analysis of experimental data [14] reported in Fig. 11 justify considering D_λ constant for $\lambda > 4$.

Adopting this consideration, Eq. (14) is analytically integrated by defining:

$$\alpha = \frac{I}{n_e F} \tag{A.5}$$

$$\beta' = \zeta\alpha \tag{A.6}$$

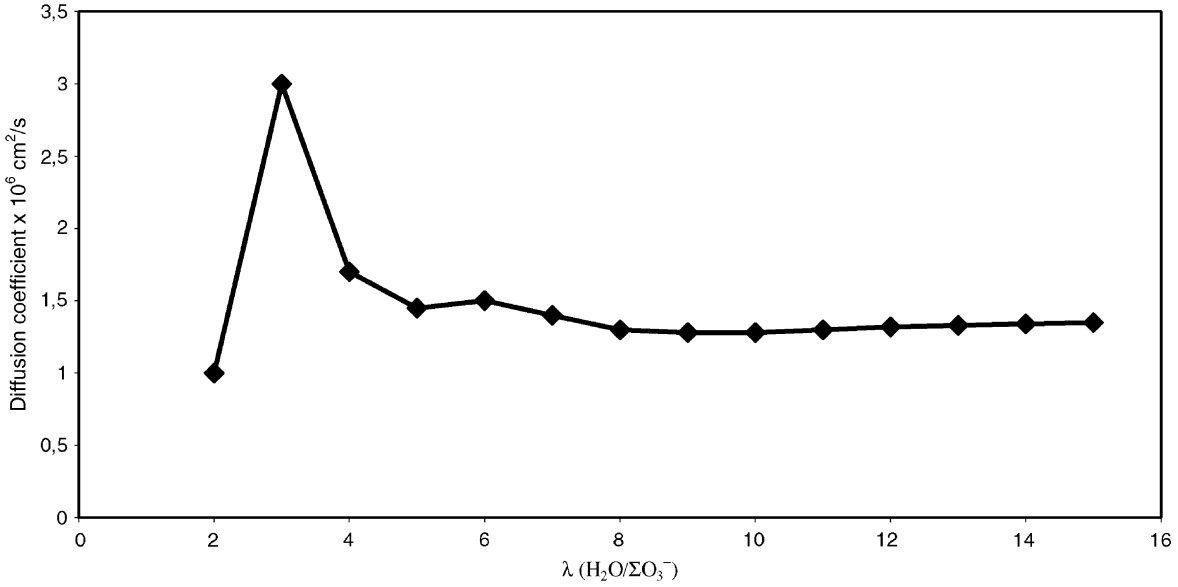

Fig. 11. Measured intradiffusion coefficient (D_λ) adapted from [16].

$$\gamma = \frac{\rho}{M} D \tag{A.7}$$

$$\delta = k\gamma \frac{3\pi\theta}{k_b T} \frac{P_c - P_a}{m} \tag{A.8}$$

$$\xi = \frac{\beta' - \delta}{\gamma} \tag{A.9}$$

Considering Eqs. (A.5)–(A.9), Eq. (14) is written as:

$$\lambda\xi - \frac{\partial\lambda}{\partial z} = \alpha\frac{\chi}{\gamma} \tag{A.10}$$

The solution of Eq. (A.10) is:

$$\lambda = \frac{\alpha\chi}{\xi\gamma}[1 - \exp(\xi z)] + \lambda_0 \exp(\xi z) \tag{A.11}$$

In addition, introducing the knowledge of the value of λ in correspondence to the electrode (i.e. $\lambda = \lambda_1$ for $z = m$) as a function of the water transport through the membrane, we obtain:

$$\chi = \frac{[\lambda_1 - \lambda_0 \exp(\xi m)]\xi\gamma}{\alpha[1 - \exp(\xi m)]} \tag{A.12}$$

The value of λ is:

$$\lambda = \frac{\lambda_1 - \lambda_0 \exp(\xi m)}{1 - \exp(\xi m)}[1 - \exp(\xi z)] + \lambda_0 \exp(\xi z) \tag{A.13}$$

So, introducing Eq. (A.13) into Eq. (14) and integrating Eq. (13) the expression of the membrane Ohmic resistance in explicit form is:

$$\Omega = \frac{\exp[\gamma(T)][f(\xi,m)]\{\xi m - \ln[(\gamma_1\lambda_1 - \gamma_2)(\exp(\xi m) - 1)] + \ln[f(\xi,m)g(\lambda_0)]\}}{\xi[\exp(\xi m)g(\lambda_0) - \lambda_1\gamma_1 + \gamma_2]} \tag{A.14}$$

where:

$$\gamma(T) = \gamma_3 \frac{\gamma_4 - T}{\gamma_4 T} \tag{A.15}$$

$$f(\xi, m) = \exp(\xi m) - 1 \tag{A.16}$$

$$g(\lambda_0) = \lambda_0\gamma_1 - \gamma_2 \tag{A.17}$$

A brief parametric analysis of Eq. (A.14) reveals that diffusivity does not strongly condition the Ohmic resistance evaluation. In fact, by differentiating Eq. (A.14), for $T = 343$ K and $P = 1.5 \times 10^5$ Pa, we obtain:

$$\frac{\partial\Omega}{\partial D_\lambda} \leq 8000 \tag{A.18}$$

and consequently

$$\Omega \leq \Omega_0 + 8000(D_\lambda - D_{\lambda_0}) \tag{A.19}$$

where Ω_0 represents the minimum value of the resistance calculated by Eq. (A.14).

In addition, the maximisation of Eq. (A.19) with the data of Fig. 11, reveals that membrane Ohmic resistance is not very sensitive to the diffusivity:

$$\Omega \leq \Omega_0 + 8000(0.5 \times 10^{-10}) \approx \Omega_0 + 0.5 \times 10^{-6} \tag{A.20}$$

The difference between the results based on this simplified approach (i.e. Eq. (A.14)) and the one obtained by the numerical integration of Eq. (A.14) (i.e. where $D_\lambda(\lambda)$) is <5%.

References

[1] S. Srinivasan, R. Mosdale, P. Stevens, C. Yang, Fuel cells: reaching the era of clean and efficient power generation in the twenty-first century, Annu. Rev. Energy Environ. 24 (1999) 281–328.

[2] E. Arato, P. Costamagna, B. Marcenaro, Control strategies of a full-size hybrid bus with second generation fuel cells, in: Proceedings of the Second International Conference on Control and Diagnostics in Automotive Applications, Genova (I), October 1998, pp. 135–144.

[3] G.H. Cole, SAE Technical Paper Series, No. 891664, Society of Automotive Engineers, 1989.

[4] M. De Francesco, E. Arato, Control strategies of the air flow rate in a PEM fuel cell hybrid bus, in: Proceedings of the Third International Conference on Control Diagnostic in Automotive Applications (CDAUTO01), Sestri Levante (I), July 2001.

[5] J.H. Hirschenhofer, D. Stauffer, R.R. Engleman, Fuel Cell. A Handbook, Version 3, DOE/METC-94/1006 (DE94004072), US Department of Fossil Energy, Morgantown Energy Technology Center, Morgantown, WV, 1994.

[6] J.C. Amphlett, R.F. Mann, B.A. Peppley, P.R. Roberge, A. Rodrigues, A model predicting transient responses of proton-exchange membrane fuel cells, J. Power Sources 61 (1996) 183–188.

[7] J.H. Lee, T.R. Lalk, A.J. Appleby, Modelling electrochemical performance in large scale proton-exchange membrane fuel cell stacks, J. Power Sources 70 (1998) 258–268.

[8] D. Thirumalai, R.E. White, Mathematical modelling of proton-exchange membrane fuel cell stacks, J. Electrochem. Soc. 144 (5) (1997) 1717–1723.

[9] J.C. Amphlett, R.F. Mann, B.A. Peppley, P.R. Roberge, A. Rodrigues, J.P. Salvador, Simulation of a 250 kW diesel fuel processor/PEM fuel cell system, J. Power Sources 71 (1998) 179–184.

[10] J.C. Amphlett, R.M. Baumert, R.F. Mann, B.A. Peppley, P.R. Roberge, A. Rodrigues, Parametric modelling of the performance of a 5 kW proton-exchange membrane fuel cell stack, J. Power Sources 49 (1994) 349–356.

[11] Y.W. Rho, S. Shrinivasan, Y.T. Kho, Mass transport phenomena in proton-exchange membrane fuel cells using O_2/He, O_2/air and O_2/N_2 mixtures. Part II. Theoretical analysis, J. Electrochem. Soc. 141 (1994) 2089–2096.

[12] P. Costamagna, Transport phenomena in polymeric membrane fuel cells, Chem. Eng. Sci. 56 (2) (2001) 323–332.

[13] D.M. Bernardi, M.W. Werbrugge, Mathematical model of a gas diffusion electrode bonded to a polymer electrolyte, AIChE J. 37 (1991) 1151–1159.

[14] T.E. Springer, M.S. Wilson, S. Gottsfeld, Modelling and experimentation diagnostics in polymer electrolyte fuel cells, J. Power Sources 140 (1993) 3513–3526.

[15] E.B. Anderson, E.J. Taylor, G. Wilemski, A. Gelb, High performance hydrogen/chlorine fuel cell for space power applications, in: Proceedings of the Fourth Space Electrochemical Research and Technology Conference, Cleveland, OH, USA, 1994, J. Power Sources 47 (3) (1994).

[16] T.E. Springer, T.A. Zawodzinski, S. Gottsfeld, Polymer electrolyte fuel cell model, J. Electrochem. Soc. 138 (8) (1991) 2334–2342.